cells

MDPI

Article

MEG3 Expression Indicates Lymph Node Metastasis and Presence of Cancer-Associated Fibroblasts in Papillary Thyroid Cancer

Sina Dadafarin [1,*], Tomás C. Rodríguez [2], Michelle A. Carnazza [3], Raj K. Tiwari [3], Augustine Moscatello [4] and Jan Geliebter [3,4,*]

[1] Department of Otolaryngology-Head and Neck Surgery, University of Washington, Seattle, WA 98195, USA
[2] RNA Therapeutics Institute, University of Massachusetts Medical School, Worcester, MA 01655, USA
[3] Department of Pathology, Microbiology and Immunology, New York Medical College, Valhalla, NY 10595, USA
[4] Department of Otolaryngology, New York Medical College, Valhalla, NY 10595, USA
* Correspondence: sinadada@uw.edu (S.D.); jan_geliebter@nymc.edu (J.G.)

Abstract: Papillary thyroid cancer is the most common endocrine malignancy, occurring at an incidence rate of 12.9 per 100,000 in the US adult population. While the overall 10-year survival of PTC nears 95%, the presence of lymph node metastasis (LNM) or capsular invasion indicates the need for extensive neck dissection with possible adjuvant radioactive iodine therapy. While imaging modalities such as ultrasound and CT are currently in use for the detection of suspicious cervical lymph nodes, their sensitivities for tumor-positive nodes are low. Therefore, advancements in preoperative detection of LNM may optimize the surgical and medical management of patients with thyroid cancer. To this end, we analyzed bulk RNA-sequencing datasets to identify candidate markers highly predictive of LNM. We identified *MEG3*, a long-noncoding RNA previously described as a tumor suppressor when expressed in malignant cells, as highly associated with LNM tissue. Furthermore, the expression of *MEG3* was highly predictive of tumor infiltration with cancer-associated fibroblasts, and single-cell RNA-sequencing data revealed the expression of *MEG3* was isolated to cancer-associated fibroblasts (CAFs) in the most aggressive form of thyroid cancers. Our findings suggest that *MEG3* expression, specifically in CAFs, is highly associated with LNM and may be a driver of aggressive disease.

Keywords: thyroid cancer; long-noncoding RNA; biomarker

Citation: Dadafarin, S.; Rodríguez, T.C.; Carnazza, M.A.; Tiwari, R.K.; Moscatello, A.; Geliebter, J. *MEG3* Expression Indicates Lymph Node Metastasis and Presence of Cancer-Associated Fibroblasts in Papillary Thyroid Cancer. *Cells* **2022**, *11*, 3181. https://doi.org/10.3390/cells11193181

Academic Editor: César López-Camarillo

Received: 7 September 2022
Accepted: 27 September 2022
Published: 10 October 2022

1. Introduction

Papillary thyroid cancer (PTC) is the most common endocrine malignancy and is the primary contributor to increasing thyroid cancer incidence [1]. While most PTC subtypes are definitively treated with thyroidectomy or lobectomy alone, more aggressive phenotypes require adjuvant radioactive iodine (RAI) therapy and/or subsequent lymph node dissection. Gene expression profiling has already demonstrated the ability to characterize nodules with indeterminate cytology [2–4], and ongoing research aims to identify predictive molecular signatures for clinically aggressive disease [5]. Indeed, a major direction for future research is the discovery of cellular factors that serve as both prognostic markers and targets for personalized therapy [5].

Lymph node metastasis occurs in approximately 40% of adult PTC cases and is associated with higher rates of recurrence and reduced survival [6–8]. Current imaging modalities, including ultrasound, CT, and FDG-PET/CT, have low sensitivities for detecting tumor-positive lymph nodes in the lateral and central compartments [9,10]. Molecular markers used as adjuvants to current imaging modalities may improve the detection of metastatic lymph nodes and better guide clinical and surgical management for these patients [11]. However, the use of single-gene mutation profiles (e.g., *BRAF*) to direct surgical management toward prophylactic cervical lymph node dissection remains controversial

and is not recommended in routine practice [5,12,13]. Preoperative biomarkers that can better predict lymph node metastasis may yet define the subset of PTC patients who would benefit most from node dissection.

Despite well-described effects on cellular function and oncogenesis, long-noncoding RNAs (lncRNAs) are relatively underutilized as biomarkers and therapeutic targets [14,15]. These transcripts of >200 nucleotides do not code for protein but have diverse regulatory potential in gene expression, alternative splicing, post-transcriptional mRNA modification, and epigenomic alterations [16–18]. Thoroughly researched lncRNAs such as *MALAT1* and *HOTAIR* [19–21] establish important roles in cancer biology and early prognostication. lncRNAs dysregulation in thyroid cancer [22] is associated with aggressive phenotypes [23,24] and stable enough to be detected in serum [25]. Thus, comprehensive identification of differentially expressed lncRNAs may expand our existing toolkit for PTC detection, grading, and staging.

Genome-wide investigations of patient PTCs have identified many lncRNAs that have potential diagnostic and therapeutic implications. The bulk of published PTC transcriptomic studies utilizes microarray and quantitative reverse transcription followed by PCR (qRT-PCR), revealing lncRNA dysregulation in cancerous tissue [26–29]. However, these methods screen for predetermined RNA variants and therefore probe only a fraction of the non-coding transcriptome [30,31]. More recently, RNA-Sequencing of small patient cohorts has associated select lncRNAs with molecular and clinical PTC subtypes [32,33]. The Cancer Genome Atlas Thyroid Carcinoma (TCGA THCA) project has reinforced these associations with larger datasets [24,34,35]; however, RNA-sequencing by TCGA was performed on polyA-purified RNA, which may not capture lncRNAs lacking poly-adenylated tails [36,37].

To maximize the detection of differentially expressed (DE) lncRNAs in PTC, we utilized our previously reported RNA-sequencing dataset of 44 matched-paired tumor and normal adjacent tissue samples using rRNA-depleted total RNA [38]. lncRNAs associated with lymph node metastasis were identified by examining modules of co-expressed genes that were associated with patients who had LNM. We found that *MEG3*, a lncRNA previously described as a tumor suppressor [39,40], was paradoxically highly associated with LNM and poor survival. We further investigated the cell-specific expression of *MEG3* in single-cell thyroid cancer data and found expression was nearly isolated to cancer-associated fibroblasts (CAFs) and that knockdown of *MEG3* in human fibroblasts downregulates the expression of matrix metalloproteases (MMPs) previously identified as contributors to cancer metastasis. Overall, our analysis identifies *MEG3* expression as highly associated with LNM in thyroid cancer with a potential role in contributing to metastatic potential via its expression in CAFs.

2. Materials and Methods

2.1. NYMC Patient Specimens

Existing specimens from 44 patients who underwent thyroidectomy with fresh frozen thyroid tissue were collected between 2009 and 2013. All tumors had corresponding matched normal-adjacent tissue, and the diagnosis of PTC was validated by pathological examination. RNA extraction, preparation, and sequencing are as previously described [38]. An R-based data object for the NYMC dataset is hosted (github.com/umasstr/NYMC-PTC, accessed on 8 August 2020) with information regarding the download and visualization of these data included.

2.2. lncRNA Annotation

Gene biotypes were obtained from GENCODE [41] and genes classified as lncRNAs had one of the following biotype annotations: 3prime_overlapping_ncRNA, antisense, bidirectional_promoter_lncRNA, lincRNA, macro_lncRNA, non_coding, processed_transcript, sense_intronic, and sense_overlapping.

2.3. BRAF Genotyping

$BRAF^{V600E}$ mutations were detected from patient samples using TaqMan probes previously described by Benlloch et al. [42]. Briefly, 100ng genomic DNA was extracted from remaining TRIzol fractions after first removing the aqueous layer containing RNA and precipitating the DNA. Forward and reverse primers, as well as mutant and wild-type probes, were designed to detect $BRAF^{V600E}$ and $BRAF^{WT}$ DNA, respectively. Primer probe sequences can be found in Supplementary Table S1. Real-time PCR was performed using the TaqMan One-Step RT-PCR Master Mix Reagents kit (Applied Biosystems, Waltham, MA, USA), and amplification and detected were performed with the ABI PRISM 7900 (Applied Biosystems, Waltham, MA, USA). BRAF mutational status was validated via manual examination of aligned RNA-Seq reads using IGV (Broad Institute, Cambridge, MA, USA).

2.4. Weighted Gene-Co-Expression Analysis (WGCNA)

We performed WGCNA [43] with 20,512 genes passing filtering and constructed co-expression gene networks using the optimal power 7 as determined by the scale-free topology criterion [44] and a minimum of 20 genes per module. Nineteen modules of co-expressed genes were constructed with a range of 33 (light yellow) to 5992 (turquoise) genes. Gene sets within each module were subject to MSigDB Hallmark Gene Set Enrichment Analysis [45] to identify biological processes common to co-expressed genes.

2.5. Fusion Detection

Fusions events were detected and annotated using a combination of STAR alignments and the STAR-SEQR tool (https://github.com/ExpressionAnalysis/STAR-SEQR, accessed on 12 June 2019). STAR-SEQR hits were filtered with the following parameters: (1) Fusion genes are only present in PTC samples; (2) at least 5 reads overlapping the cross junction must be present; (3) fused genes must be translocated from different chromosomes, or genomic distance between the genes must be >150 kb. RT-PCR followed by gel electrophoresis was performed to validate filtered hits. Fusion details and primer sequences used are provided in Supplemental Table S2.

2.6. TCGA Data

Level three RNA-Seq data were downloaded from the UCSC Xena Browser [46].

2.7. Pathway and GO Enrichment Analysis

KEGG Pathway and Gene Ontology enrichment analyses were performed on Advaita's iPathwayGuide (http://www.advaitabio.com/ipathwayguide, accessed on 6 June 2019) platform using DE genes (abs(log2FC) > 1.5 and q-value < 0.05). Statistical tests of pathway and GO term enrichment were adjusted using FDR correction.

2.8. Thyroid Differentiation Score and ERK Signature

We calculated the thyroid differentiation score using 16 thyroid metabolism and function genes first characterized by TCGA THCA study [47].

$$TDS = Average[Log2(FC)] \text{ across 16 genes}$$

MAPK signaling activity was measured using the ERK signature score from TCGA using 52 MAPK signaling genes first described by Pratilas et al. [48].

$$ERK\ score = log2 \sum_{n=1}^{52} [(median(RSEM_n all\ patients) - (RSEM_n individual\ patient)]/52$$

2.9. Statistical Analysis

Hierarchical clustering, heatmap generation, Spearman, and Pearson correlation analyses of DEGs were performed on R version 3.5.3. Pearson's chi-square test or Fisher's exact

test (when samples were <5) was used to analyze categorical variables. The R package pheatmap (http://rpackages.ianhowson.com/cran/pheatmap/, accessed 10 January 2021) was used for heatmap generation and hierarchical clustering.

2.10. Estimating Tumor Infiltration with CAFs Using TIMER2.0

We used TIMER2.0 [49] to investigate the correlation between *MEG3* expression and infiltration of CAFs in the TCGA THCA dataset. "Purity Adjustment" option was selected to account for the confounding effect of tumor purity and immune cell type infiltration.

2.11. Single-Cell Anaplastic Thyroid Cancer Data

Single-cell data from 5 previously described anaplastic thyroid cancer samples [50] were analyzed using the CancerSCEM webtool [51].

3. Results

3.1. Clinical Characteristics of PTC Cohort

We analyzed transcriptomic data from 44 PTC samples with matched normal adjacent tissue (NAT) collected from patients undergoing thyroidectomy between 2009 and 2013 as part of the NYMC dataset [38]. Most patients in this cohort had indicators of aggressive disease, including high rates of $BRAF^{V600E}$ mutation (80%), capsular invasion (77.8%), multifocality (88.9%), and higher T stage (75.6% T3 or higher) (Table 1). Previous studies of PTC epidemiology report $BRAF^{V600E}$ mutations present in 40–60% of PTC cases [52,53], although after reclassification separating the follicular variant PTC (FVPTC) from classical PTC (cPTC), Yoo et al. found 71.4% of cPTC harbored BRAF mutations and more aggressive phenotypes compared to other subtypes [54]. Clinicopathological characteristics of the NYMC dataset showed no significant difference in age, tumor size, lymph node metastasis, or extracapsular invasion when comparing $BRAF^{V600E}$ and $BRAF^{WT}$ tumors, although statistical analysis may be impacted by the limited number of $BRAF^{WT}$ tumors.

Table 1. Patient demographic and clinicopathological characteristics.

	BRAFV600E	BRAFWT	Total	*p*-Value
N	36 (80%)	9 (20%)	44	
Age	47.8 (20–76)	49 (34–60)	48 (20–76)	0.41
Female sex	26 (72%)	8 (89%)	34 (76%)	0.65
Thyroiditis	17 (47%)	5 (56%)	22 (49%)	0.72
Tumor size	1.9 cm (0.45–4.3 cm)	1.7 cm (0.9–3.2 cm)	2.8 cm (0.45–4.3 cm)	0.54
Lymph node metastasis	15 (42%)	4 (44%)	19 (42%)	1
Invasion	27 (75%)	7 (77%)	34 (76%)	1
T stage				1
T1–T2	9 (25%)	2 (22%)	11 (24%)	
T3–T4	27 (75%)	7 (77%)	34 (76%)	

3.2. Analysis of Tumor vs. Normal Transcriptomics

Principal component analysis (PCA) on all specimens demonstrated distinct separation on the PC2 axis between PTC and normal adjacent tissue (Figure 1A). Next, we measured thyroid cell differentiation and activation of the MAPK signaling pathway using scoring methods developed by TCGA: the thyroid differentiation score (TDS) and ERK score (Figure 1C) [47]. Consistent with results from the TCGA and Song et al. 2018 [55], $BRAF^{V600E}$-mutant PTC scored lower on the TDS compared to $BRAF^{WT}$ tumors ($p = 4.5 \times 10^{-6}$). Furthermore, $BRAF^{V600E}$ mutant samples displayed varying TDS scores ranging from −0.48 to −3.48, representing high and low differentiation, respectively, while the TDS of $BRAF^{WT}$ tumors ranged from –0.029 to –1.81. The ERK score, which represents no clear distinction was made between male and female tumors based on BRAF status, ERK score, or TDS (Figure 1C). KEGG pathway enrichment analysis of differentially expressed (DE) genes identified cell adhesion molecules and ECM-receptor interaction as well as

pathways related to host immune function (Cytokine–cytokine receptor interactions and allograft rejection) as the most highly enriched among the NYMC dataset (Figure 1D). These findings are consistent with those by Song and colleagues that showed cell adhesion molecules and ECM-receptor interaction pathways were enriched among upregulated genes in PTC [55].

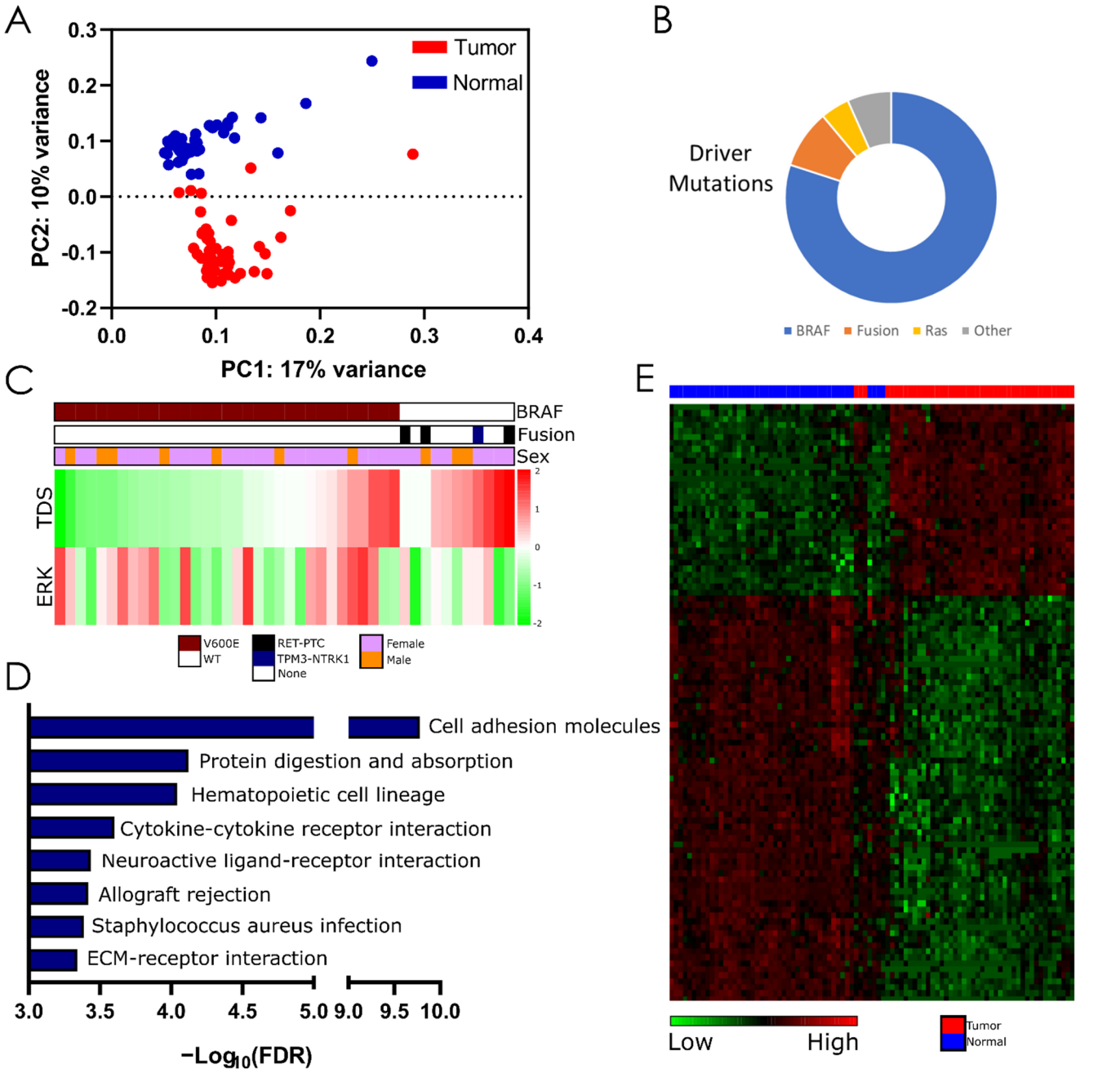

Figure 1. Differential expression analysis between tumor and normal thyroid tissue. (**A**) Principal component analysis of 44 PTC and matched normal tissue. (**B**) Proportion of known driver mutations identified in tumor samples. (**C**) Mutational status, sex, TDS, and ERK score in individual tumors. TDS and ERK scale represent Log2-scaled high and low thyroid differentiation and ERK-activation based on gene signatures [47]. (**D**) Pathway analysis of differentially expressed genes. (**E**) Hierarchical clustering of the top 100 differentially expressed lncRNAs (scaled normalized reads by column). FDR, false discovery rate; TDS, thyroid differentiation score.

Four *BRAF*^{WT} PTC tumors harbored fusion genes: *CCDC6-RET*, *TRIM27-RET*, *ACBD5-RET,* and *TPM3-NTRK1*. Validated fusion genes, breakpoint regions, and expression levels are available in Supplementary Table S2. All four fusion genes were previously reported in PTC [47,54,56,57].

3.3. WGCNA Identifies a Gene Co-Expression Module Associated with LNM

lncRNAs play a key role in transcriptional regulation of protein-coding genes [58], though often in complex genetic circuits not easily reconciled with clinical phenotypes. Our analysis of the NYMC dataset identified 756 non-coding RNAs that underwent ≥1.5-fold change between tumor and normal (q-value ≤ 0.05) (Figure 1E). To identify lncRNAs related to available sample characteristics, we constructed 19 gene network modules from pairwise expression correlations of 20,512 coding and non-coding genes using WCGNA. Modules underwent MSigDB Hallmark Gene Set enrichment analysis, and their eigengenes (the first principal component of each module) were associated with clinicopathological features (Figure 2A). Among the clinical traits probed, lymph node metastasis (LNM) showed the strongest association to a gene module (black, $p = 0.05$). In total, 188 genes were upregulated and 482 were downregulated in the black module and hallmark pathways enriched included epithelial–mesenchymal transition ($p = 1.33 \times 10^{-81}$), TNFα Upregulation ($p = 2.03 \times 10^{-43}$), and Hypoxia ($p = 1.82 \times 10^{-17}$) (Figure 2B). Several genes that were previously shown to contribute to aggressive phenotypes in thyroid cancer, including SERPINE1 and TBX15 [59,60], were identified in this module and significantly correlated with LNM (Supplementary Table S3). We did not appreciate a gene cluster among black modules genes that would distinguish LNM+ and LNM- tumors (Figure 2C).

Among the 74 lncRNAs co-expressed within the black (LNM) module, we examined those with the largest Gene Significance score (GS) (Table 2). Among these lncRNAs, *LINC00346*, *CASC15, EGFR-AS1*, *DIO3OS,* and *LINC00702* were all previously reported to contribute to proliferation and invasion [61–64]. Interestingly, we identified *NBAT1,* a tumor suppressor gene in other cancer types [65], in the LNM module. Five lncRNAs were differentially expressed only in tumors with LNM; however, the fold change between tumor and normal was only significantly greater among LNM-positive tumors for *NBAT1, RP11-815J21.4,* and *RP11-106D4* (Figure 2D).

Table 2. Top 15 differentially expressed black module lncRNAs.

Gene Name	GS.LN	p*.GS.LN	MM.black	p.MM.black
LINC00346	0.395204	0.009589	0.623782	1.02×10^{-05}
RP1-79C4.4	0.383766	0.01211	0.760822	4.99×10^{-09}
RP5-1071N3.1	0.381124	0.012767	0.306905	0.048048
AC159540.2	0.31683	0.040921	0.290224	0.062257
MEG3	0.316771	0.040961	0.91168	4.85×10^{-17}
NBAT1	0.308945	0.046506	0.682119	6.54×10^{-07}
RP11-124N14.3	0.30859	0.046772	0.502946	0.000687
ITPK1-AS1	0.29417	0.058626	0.362727	0.018234
CASC15	0.287496	0.06487	0.68056	7.09×10^{-07}
EGFR-AS1	0.267027	0.087358	0.213671	0.174238
DIO3OS	0.262486	0.093083	0.700355	2.43×10^{-07}
DNM3OS	0.26201	0.093699	0.588983	4.07×10^{-05}
LINC00702	0.257338	0.099919	0.66197	1.81×10^{-06}
TEX26-AS1	0.254926	0.10325	0.690438	4.20×10^{-07}
RP11-273B20.1	0.25004	0.11026	0.585077	4.71×10^{-05}

GS, gene significance; MM, module membership, which indicates Pearson correlation between gene expression and module eigengene. * *p.* denotes correlation coefficient *p*-value.

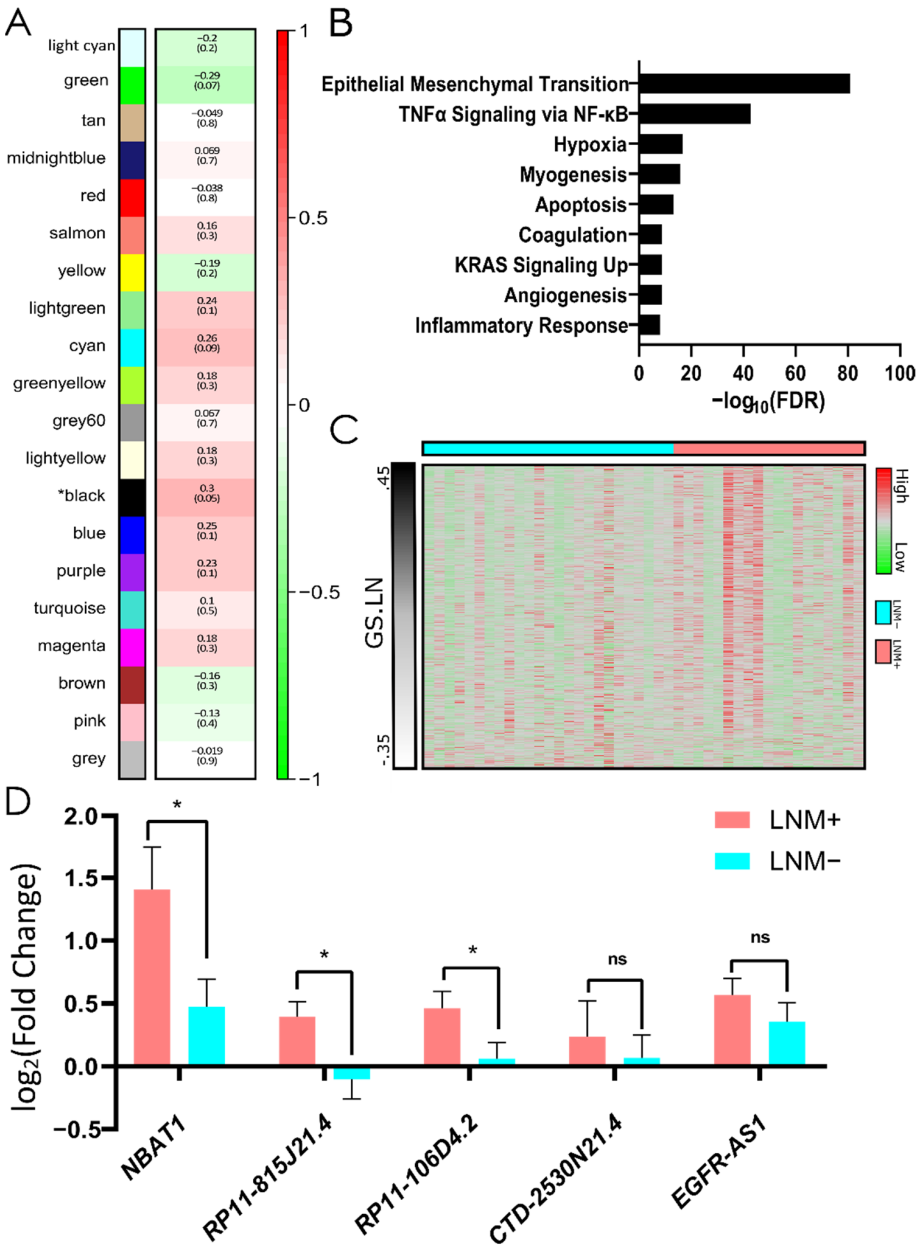

Figure 2. LNM-related co-expression analysis of PTC samples. (**A**) Relationship between WCGNA modules and LNM status. Values represent Pearson correlation coefficient and the correlation *p*-value (in brackets) between LNM and module eigengene. (**B**) Hallmark gene set analysis of the module most correlated with LNM status (black). (**C**) Black module constituent gene expression ranked by gene significance value related to lymph node metastasis (GS.LN) (**D**) Black module lncRNAs upregulated in LNM+ tissue but not LNM- tissue. LNM+ and LNM−, positive and negative lymph node status. * $p < 0.05$; ns, non-significant.

Ranked by module membership (MM) score denoting correlation between gene expression and eigengene, black module constituent, *MEG3*, was most predictive of LNM. Kaplan–Meyer analysis of *MEG3* in the TCGA shows lower overall survival in patients with higher expression of *MEG3*; this effect intensifies in BRAF mutant patients (Figure 3A). We also examined TCGA PTC transcriptomes and found that *MEG3* is expressed higher in metastatic tumors compared to normal, though the former is poorly represented in this study ($n = 8$) (Figure 3B). Using qPCR, Wang et al. [66] found *MEG3* to be downregulated in LNM-positive PTC patient samples and that overexpression of *MEG3* reduces migration and invasion in vitro via *RAC1* inhibition. In contrast, our RNA-seq data show that *MEG3* is

downregulated in LNM-negative samples (q-value = 0.0045) and expression is unchanged in LMN-positives (q-value = 0.86) (Figure 3C). We hypothesized that qPCR transcript quantification may not capture the full library of *MEG3* lncRNA variants expressed in PTC. To reconcile discordant trends in tumor *MEG3* expression obtained by qPCR [66] and RNA-Seq, we surveyed all *MEG3* isoforms found in at least 50% of samples in our dataset. Five isoforms (ENST00000455531, ENST00000398460, ENST00000522771, ENST00000398461 and ENST00000452120) passed filtering criteria. ENST00000452120 displayed the highest overall expression in tumor and normal tissue, was significantly downregulated in LMN-negative tumors, and showed higher (non-significant, $p = 0.2$) expression in LMN-positive tumors. No obvious isoform switch of the *MEG3* gene was observed between LNM-positive, LNM-negative, and normal samples (Figure 4A). Furthermore, Wang et al. qPCR probes showed no enrichment bias toward any subset of *MEG3* isoforms (Supplementary Figure S1).

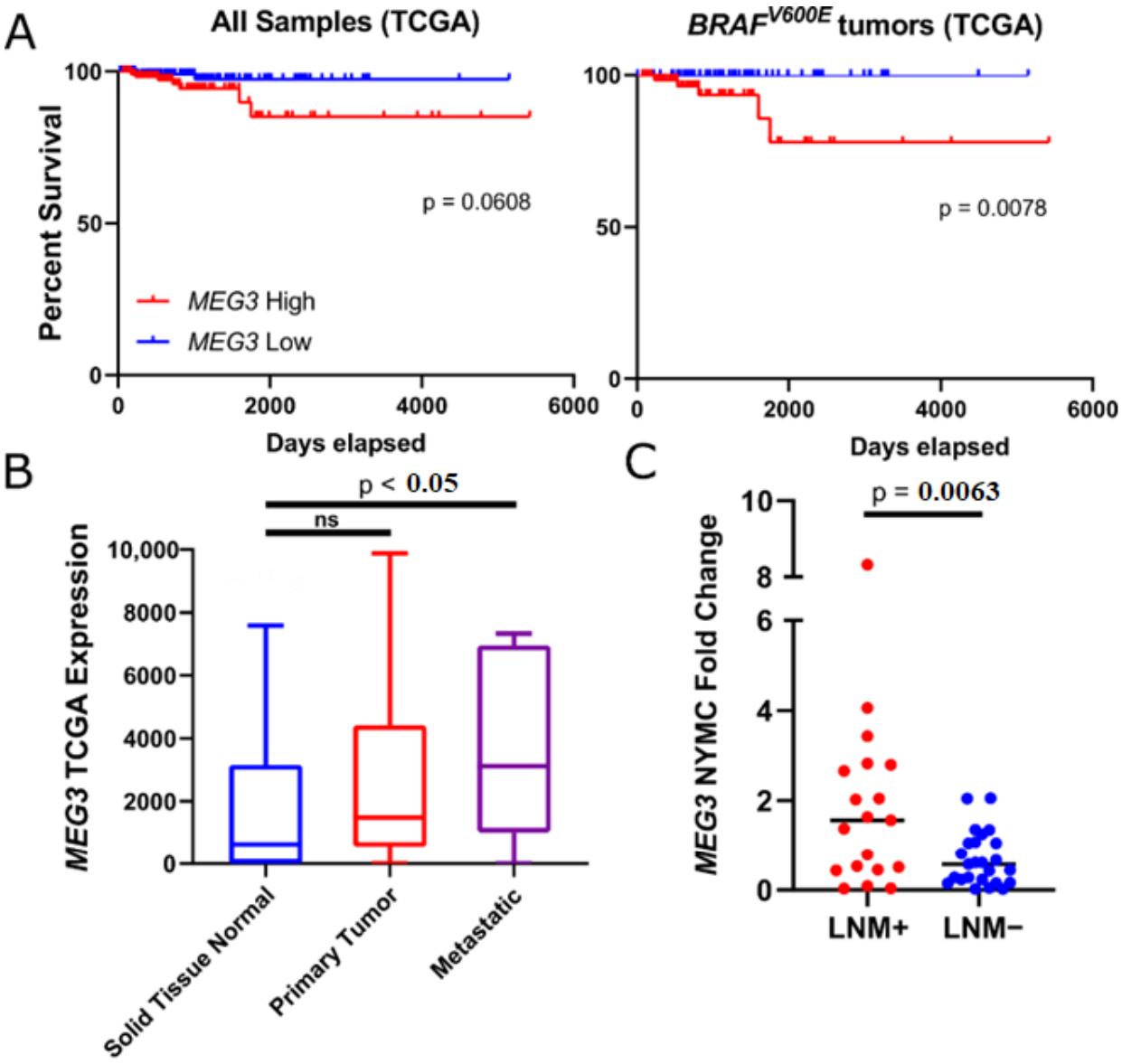

Figure 3. *MEG3* expression is increased in PTC with LNM and correlates with poor outcomes (**A**) TCGA all patients (left) and $BRAF^{V600E}$ cohort (right) survival given top (red) and bottom (blue) quartile *MEG3* expression. (**B**) TCGA Solid Tissue Normal *MEG3* expression. (**C**) *MEG3* fold-change expression in NYMC LNM+ and LNM-PTC.

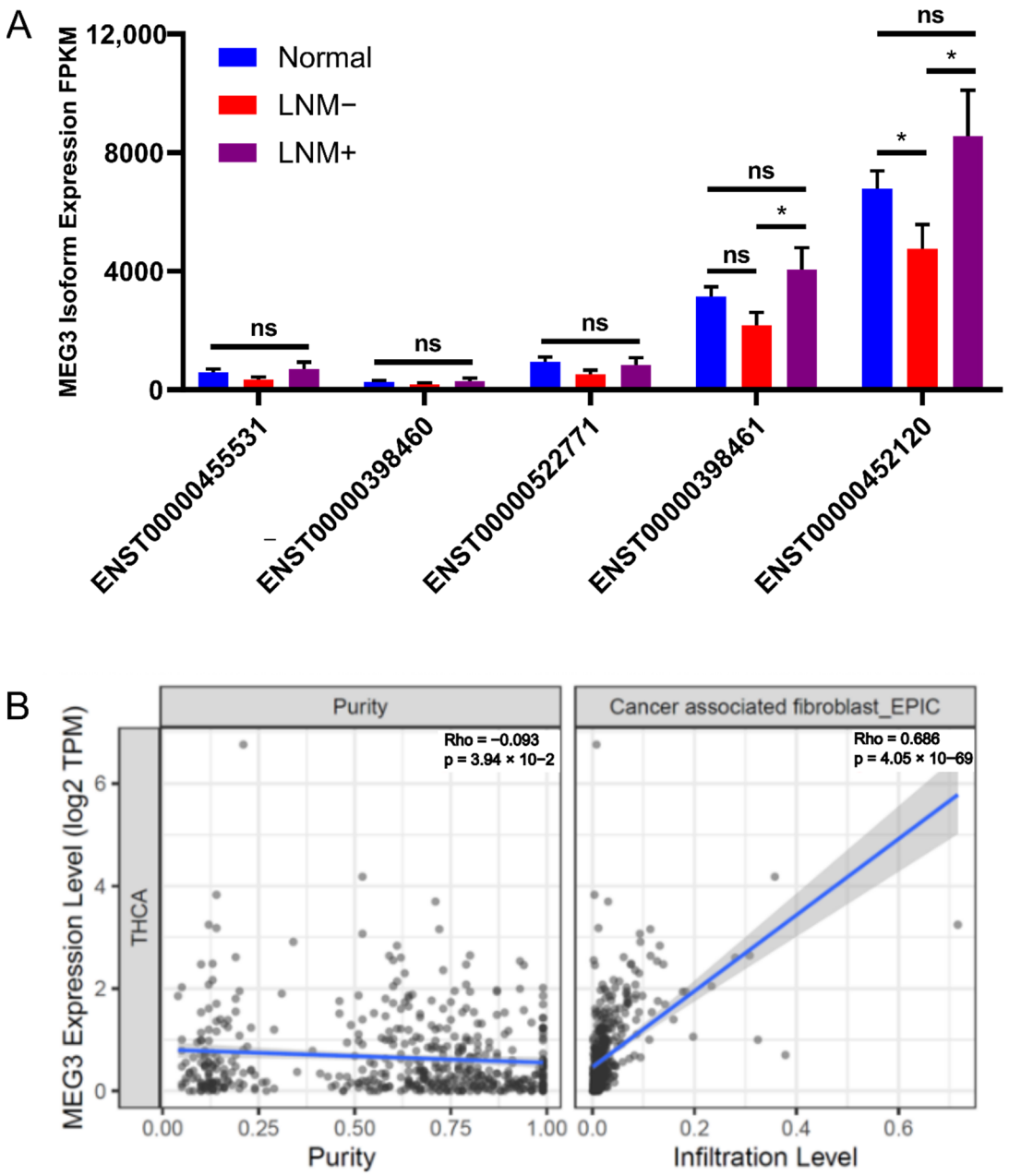

Figure 4. *MEG3* isoform expression and association with infiltration of CAFs. (**A**) *MEG3* transcript isoform usage in normal (non-cancerous) tissue and NYMC PTC (LNM+/−). (**B**) Scatter plots demonstrating the correlation of *MEG3* expression in TCGA THCA project with tumor purity and estimated infiltration level of CAFs using TIMER2.0. EPIC output was used to represent fibroblast infiltration estimates from TIMER2.0. * $p < 0.05$; ns, non-significant.

The study by Wang et al. used immortalized PTC cell lines in monoculture to study the role of *MEG3* in invasion and metastasis. A potential reason for the discrepancy between that study's results and our findings from the TCGA and NYMC dataset is that *MEG3* plays unique roles in cell-autonomous mechanisms vs. its contribution to the tumor microenvironment. Tumors often recruit or modify members of the microenvironment, such as infiltrating immune cells, vascular endothelial and smooth muscle cells, and fibroblasts, to promote metastatic progression [67,68]. We therefore used TIMER2.0 to investigate the correlation between *MEG3* expression in the TCGA dataset and infiltration across cell types in the tumor microenvironment. Cancer-associated fibroblasts were strongly associated with *MEG3* expression across all four deconvolution algorithms that can measure this

cell type (Figure 4B). Given this high correlation, we hypothesized that *MEG3*-expressing tumors may be secreting cytokines that recruit and activate tumor fibroblasts, including members of the TGFβ superfamily and PDGFα/β. Therefore, we calculated the Pearson correlation between *MEG3* expression and these cytokines in our tumor samples and found TGFβ3 to be the most significantly associated with *MEG3* expression (Pearson's rho = 0.74).

To determine the cell type within the thyroid cancer tumor environment that expresses *MEG3*, we aimed to use existing single-cell RNA-sequencing (scRNA-Seq) data from thyroid cancer samples with high metastatic and invasive potential. We therefore examined five anaplastic thyroid cancer samples, given they are the most aggressive form of thyroid cancer that frequently originates from the context of dedifferentiating PTC [69]. We found that four out of five samples showed that expression of *MEG3* was nearly isolated to CAFs (Figure 5). Furthermore, the only sample lacking *MEG3* expression had the highest cellular purity as scored, suggesting the single-cell suspension of this sample may be enriched with malignant cells and therefore lack sufficient CAFs to detect *MEG3* expression (Supplemental Table S4).

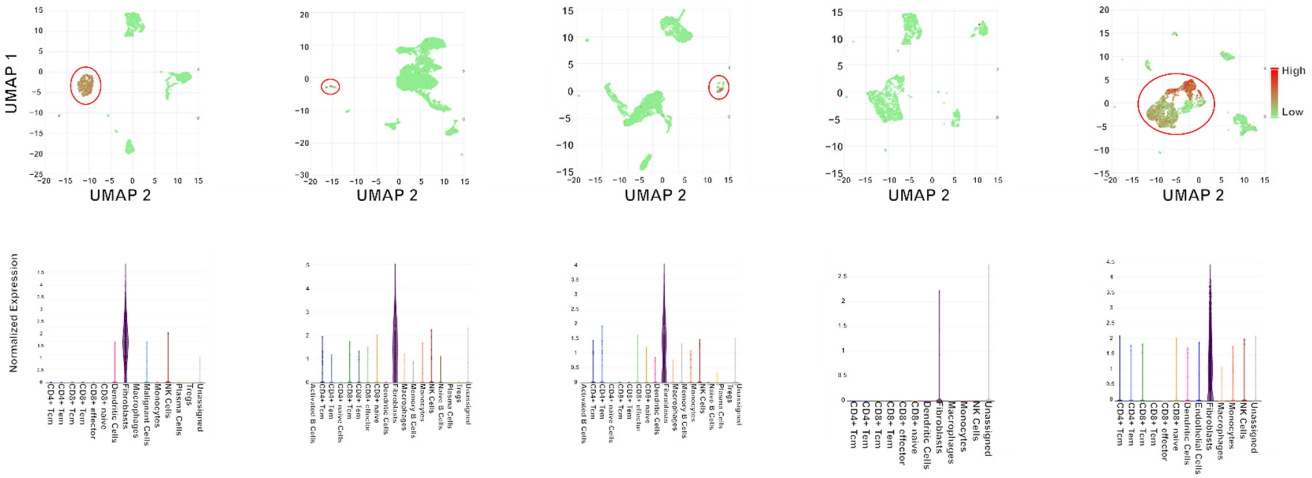

Figure 5. Single-cell RNA-sequencing results identify cell types that express *MEG3*. Expression profile of *MEG3* in 5 ATC patient tumors represented as UMAPs with overlaid heatmaps demonstrating *MEG3* expression and expression in different cell subtypes in each sample. Red circles represent clusters of cells that are annotated as fibroblasts.

From the single-cell data we examined, there was clear heterogeneity in the expression of *MEG3* among tumor-associated fibroblasts. To better understand functionally how *MEG3*-expressing fibroblasts differed from those lacking *MEG3* expression, we examined gene expression data of human fibroblasts with *MEG3* experimentally downregulated. We examined published data from Mondal and colleagues who performed RNA microarrays on human fibroblasts treated with *MEG3* siRNAs [70]. Among genes significantly downregulated by *MEG3* knockdown, as determined by a −2 fold-change from *MEG3*-knockdown to control, were MMP-1, MMP-9, and MMP-16, three metalloproteases with previously characterized roles in tumor metastasis [71–73].

4. Discussion

Despite a generally favorable prognosis, papillary thyroid cancer can transition into aggressive subtypes and metastatic disease in select patients. A toolkit of pharmaceutical, surgical, and targeted radiation-based therapies has extended longevity of these individuals; however, it remains unclear which patients will benefit most from a given intervention in the setting of advanced PTC. As molecular profiling technologies—most prominently high-throughput sequencing—become cheaper and more accessible, novel genetic hallmarks in PTC could inform the clinical approach. In particular, the detection of LNM in the central

and lateral neck compartments in the preoperative setting potentially alters the surgical management of patients [74,75].

Here, we analyzed a large set of PTC transcriptomes with a focus on lncRNAs, given their increasingly recognized role in a variety of cancer-related processes yet underutilization as biomarkers relative to protein-coding genes [17,76,77]. We sought to enrich lncRNAs tied to aggressive features of PTC. Using WGCNA, we identified a module of 729 genes associated with epithelial–mesenchymal transition that exhibits a strong correlation to LNM-positivity. Most notably, the lncRNA *MEG3* was determined to have the highest module membership score, indicating it may be highly interconnected within this co-expression module as a potential hub gene. We further found increased *MEG3* expression in PTC to be associated with LNM, worse overall survival, and higher infiltration with CAFs.

MEG3 has been described as a tumor suppressor in many cancer types, including glioma, hepatocellular carcinoma, and even thyroid cancer [39,66,78,79]. However, these studies relied on the expression of *MEG3* in tumor cell lines, bulk tissue with predominantly malignant cells, and animal models derived from xenografts of primary tumors. More recent investigations of the tumor microenvironment via single-cell technologies have started to show a diverse role of *MEG3* depending on its cellular context. Pan and colleagues demonstrated using scRNA-seq of pancreatic ductal carcinomas that *MEG3* expression was significantly enriched in CAFs of primary tumors, and *MEG3* expression was significantly associated with epithelial-mesenchymal transition signatures [80]. Given our finding that the proportion of CAFs was highly associated with *MEG3* expression in our bulk tumor samples, we aimed to determine if the *MEG3* was being expressed by tumor cells that were recruiting CAFs, or if CAFs were directly expressing *MEG3*. To determine the cell types that express *MEG3* in aggressive thyroid cancer, we analyzed existing scRNA-seq data from anaplastic thyroid cancer. Four out of five samples demonstrate *MEG3* expression in CAFs but little expression in tumor cells, suggesting CAFs are the primary cell types expressing *MEG3*.

We reasoned that the presence of *MEG3*-expressing CAFs drives metastatic potential through reorganization of the extracellular matrix to drive tumor invasion. We therefore examined gene expression data for *MEG3*-knockdown in human fibroblasts. MMP-1, MMP-9, and MMP-16 were downregulated in *MEG3*-knockdown fibroblasts, suggesting *MEG3* regulates the expression of these metalloproteases with implications in CAF-driven metastasis. Mondal and colleagues showed that *MEG3* regulates gene expression by targeting chromatin regions and forming RNA-DNA triplex structures at distal regulatory elements and recruiting polycomb repressive complex 2 (PRC2) to inhibit expression [70]. Interestingly, *MEG3* was shown to downregulate TGFβ receptor 1 in fibroblasts by Mondal, which may appear discordant with our finding CAFs expressing *MEG3* are associated with LNM-positive thyroid cancer since TGFβ signaling is needed for fibroblast activation. However, one possibility is that *MEG3* expression may be downstream of TGF B-signaling and a component of the negative feedback loop of the TGFβ signaling cascade [81]. Furthermore, Terashima and colleagues demonstrated that *MEG3* knockdown inhibits TGFβ-induced EMT in lung cancer cell lines [82]. A study of *MEG3* expression in idiopathic pulmonary fibrosis using scRNA-seq demonstrated that *MEG3* regulates the differentiation of bronchial cells through diverse mechanisms, including through *YAP1, NOTCH,* and *SOX2* signaling [83]. Future functional studies are needed to further determine the biological role of *MEG3* in CAF activation and its potential contribution to invasion and metastasis.

A key limitation of our study is that normal adjacent tissue while carrying histologic features such as healthy tissue have distinct gene expression patterns and may represent an intermediate state or the effects of field cancerization [83]. A recent analysis of adjacent tissue and healthy donor tissue across eight tumor types, including thyroid cancer, found a majority of differentially expressed genes between tumor and adjacent tissue overlaps with gene differentially expressed between tumors and healthy donor tissue, and a limited number of genes showed discordant patterns of differential expression [84]. Nevertheless,

future studies should validate coding and non-coding transcripts that we identified in this study by comparing healthy thyroid tissue to PTC.

In conclusion, we utilized multiple transcriptomic datasets with matched-paired controls for the identification of lncRNA in a gene co-expression network associated with LNM and enriched in epithelial–mesenchymal transition gene set. The lncRNA *MEG3* was identified as a hub of this co-expression module and an indicator of LNM and CAFs infiltration. The identification of *MEG3*-expressing CAFs rather than malignant cells via scRNA-seq suggests this lncRNA may be playing unique roles in tumorigenesis, invasion, and metastasis based on the cellular context. However, further investigation is needed to fully elucidate the diverse mechanisms *MEG3* has and its potential use in personalizing management for PTC.

Supplementary Materials: The following supporting information can be downloaded at: https://www.mdpi.com/article/10.3390/cells11193181/s1, Figure S1: Gencode annotated *MEG3* isoforms and qPCR primer pair used by Wang et al.; Tables S1–S4.

Author Contributions: Conceptualization by S.D., R.K.T., A.M. and J.G.; methodology by S.D., T.C.R. and J.G.; software S.D. and T.C.R.; validation by S.D. and M.A.C.; writing—original draft preparation by S.D.; writing—review and editing by S.D., T.C.R. and J.G.; supervision by R.K.T., A.M. and J.G.; funding acquisition by R.K.T., A.M. and J.G. All authors have read and agreed to the published version of the manuscript.

Funding: This research was funded by the New York State Empire Clinical Research Investigator Program (ECRIP 2014, awardee Jan Geliebter) and the Department of Otolaryngology at New York Medical College.

Institutional Review Board Statement: This study was approved by the institutional review board of New York Medical College in accordance with the Declaration of Helsinki. All TCGA and single-cell RNA sequencing data used in this study were downloaded from publicly available sources.

Informed Consent Statement: Written informed consent was obtained from each patient.

Data Availability Statement: Level three RNA-Seq data were downloaded from the UCSC Xena Browser [46]. Single-cell RNA-seq data were obtained using the CancerSCEM webtool [51].

Acknowledgments: We wish to thank Sarnath Singh for providing technical support, Codrin Iacob for guidance in preparing tissue samples, and Monica Schwarcz and Stimson Schantz and members of the Tiwari laboratory for providing discussion and feedback related to this work.

Conflicts of Interest: The authors declare no conflict of interest. The funders had no role in the design of the study; in the collection, analyses, or interpretation of data; in the writing of the manuscript; or in the decision to publish the results.

References

1. Davies, L.; Welch, H.G. Current Thyroid Cancer Trends in the United States. *JAMA Otolaryngol. Head Neck Surg.* **2014**, *140*, 317–322. [CrossRef]
2. Endo, M.; Nabhan, F.; Porter, K.; Roll, K.; Shirley, L.A.; Azaryan, I.; Tonkovich, D.; Perlick, J.; Ryan, L.E.; Khawaja, R.; et al. Afirma Gene Sequencing Classifier Compared with Gene Expression Classifier in Indeterminate Thyroid Nodules. *Thyroid* **2019**, *29*, 1115–1124. [CrossRef]
3. Patel, K.N.; Angell, T.E.; Babiarz, J.; Barth, N.M.; Blevins, T.; Duh, Q.-Y.; Ghossein, R.A.; Harrell, R.M.; Huang, J.; Kennedy, G.C.; et al. Performance of a Genomic Sequencing Classifier for the Preoperative Diagnosis of Cytologically Indeterminate Thyroid Nodules. *JAMA Surg.* **2018**, *153*, 817–824. [CrossRef]
4. Marti, J.L.; Avadhani, V.; Donatelli, L.A.; Niyogi, S.; Wang, B.; Wong, R.J.; Shaha, A.R.; Ghossein, R.A.; Lin, O.; Morris, L.G.T.; et al. Wide Inter-Institutional Variation in Performance of a Molecular Classifier for Indeterminate Thyroid Nodules. *Ann. Surg. Oncol.* **2015**, *22*, 3996–4001. [CrossRef]
5. Haugen, B.R.; Alexander, E.K.; Bible, K.C.; Doherty, G.M.; Mandel, S.J.; Nikiforov, Y.E.; Pacini, F.; Randolph, G.W.; Sawka, A.M.; Schlumberger, M.; et al. 2015 American Thyroid Association Management Guidelines for Adult Patients with Thyroid Nodules and Differentiated Thyroid Cancer: The American Thyroid Association Guidelines Task Force on Thyroid Nodules and Differentiated Thyroid Cancer. *Thyroid* **2016**, *26*, 1–133. [CrossRef]
6. Mazzaferri, E.L. Management of a Solitary Thyroid Nodule. *N. Engl. J. Med.* **1993**, *328*, 553–559.

7. Mazzaferri, E.L.; Jhiang, S.M. Long-Term Impact of Initial Surgical and Medical Therapy on Papillary and Follicular Thyroid Cancer. *Am. J. Med.* **1994**, *97*, 418–428. [CrossRef]
8. Podnos, Y.D.; Smith, D.; Wagman, L.D.; Ellenhorn, J.D.I. The Implication of Lymph Node Metastasis on Survival in Patients with Well-Differentiated Thyroid Cancer. *Am. Surg.* **2005**, *71*, 731–734. [CrossRef]
9. Ahn, J.E.; Lee, J.H.; Yi, J.S.; Shong, Y.K.; Hong, S.J.; Lee, D.H.; Choi, C.G.; Kim, S.J. Diagnostic Accuracy of CT and Ultrasonography for Evaluating Metastatic Cervical Lymph Nodes in Patients with Thyroid Cancer. *World J. Surg.* **2008**, *32*, 1552–1558. [CrossRef]
10. Jeong, H.-S.; Baek, C.-H.; Son, Y.-I.; Choi, J.-Y.; Kim, H.-J.; Ko, Y.-H.; Chung, J.-H.; Baek, H.-J. Integrated 18F-FDG PET/CT for the Initial Evaluation of Cervical Node Level of Patients with Papillary Thyroid Carcinoma: Comparison with Ultrasound and Contrast-Enhanced CT. *Clin. Endocrinol.* **2006**, *65*, 402–407. [CrossRef]
11. Xia, S.; Wang, C.; Ni, X.; Ni, Z.; Dong, Y.; Zhan, W. NONHSAT076754 Aids Ultrasonography in Predicting Lymph Node Metastasis and Promotes Migration and Invasion of Papillary Thyroid Cancer Cells. *Oncotarget* **2017**, *8*, 2293–2306. [CrossRef]
12. Han, P.A.; Kim, H.-S.; Cho, S.; Fazeli, R.; Najafian, A.; Khawaja, H.; McAlexander, M.; Dy, B.; Sorensen, M.; Aronova, A.; et al. Association of BRAF V600E Mutation and MicroRNA Expression with Central Lymph Node Metastases in Papillary Thyroid Cancer: A Prospective Study from Four Endocrine Surgery Centers. *Thyroid* **2016**, *26*, 532–542.
13. Dutenhefner, S.E.; Marui, S.; Santos, A.B.O.; de Lima, E.U.; Inoue, M.; Neto, J.S.B.; Shiang, C.; Fukushima, J.T.; Cernea, C.R.; Friguglietti, C.U.M. BRAF: A Tool in the Decision to Perform Elective Neck Dissection? *Thyroid* **2013**, *23*, 1541–1546. [CrossRef]
14. Mercer, T.R.; Dinger, M.E.; Mattick, J.S. Long Non-Coding RNAs: Insights into Functions. *Nat. Rev. Genet.* **2009**, *10*, 155–159. [CrossRef]
15. Ponting, C.P.; Oliver, P.L.; Reik, W. Evolution and Functions of Long Noncoding RNAs. *Cell* **2009**, *136*, 629–641. [CrossRef]
16. Lee, J.T. Epigenetic Regulation by Long Noncoding RNAs. *Science* **2012**, *338*, 1435–1439. [CrossRef]
17. Huarte, M. The Emerging Role of lncRNAs in Cancer. *Nat. Med.* **2015**, *21*, 1253–1261. [CrossRef]
18. Tripathi, V.; Ellis, J.D.; Shen, Z.; Song, D.Y.; Pan, Q.; Watt, A.T.; Freier, S.M.; Bennett, C.F.; Sharma, A.; Bubulya, P.A.; et al. The Nuclear-Retained Noncoding RNA MALAT1 Regulates Alternative Splicing by Modulating SR Splicing Factor Phosphorylation. *Mol. Cell* **2010**, *39*, 925–938. [CrossRef]
19. Zhang, Y.; Yu, S.; Jiang, L.; Wang, X.; Song, X. HOTAIR Is a Promising Novel Biomarker in Patients with Thyroid Cancer. *Exp. Ther. Med.* **2017**, *13*, 2274–2278. [CrossRef]
20. Rinn, J.L.; Kertesz, M.; Wang, J.K.; Squazzo, S.L.; Xu, X.; Brugmann, S.A.; Goodnough, L.H.; Helms, J.A.; Farnham, P.J.; Segal, E.; et al. Functional Demarcation of Active and Silent Chromatin Domains in Human HOX Loci by Noncoding RNAs. *Cell* **2007**, *129*, 1311–1323. [CrossRef]
21. Ji, P.; Diederichs, S.; Wang, W.; Böing, S.; Metzger, R.; Schneider, P.M.; Tidow, N.; Brandt, B.; Buerger, H.; Bulk, E.; et al. MALAT-1, a Novel Noncoding RNA, and Thymosin beta4 Predict Metastasis and Survival in Early-Stage Non-Small Cell Lung Cancer. *Oncogene* **2003**, *22*, 8031–8041. [CrossRef] [PubMed]
22. Sedaghati, M.; Kebebew, E. Long Noncoding RNAs in Thyroid Cancer. *Curr. Opin. Endocrinol. Diabetes Obes.* **2019**, *26*, 275–281. [CrossRef] [PubMed]
23. Cui, M.; Chang, Y.; Du, W.; Liu, S.; Qi, J.; Luo, R.; Luo, S. Upregulation of lncRNA-ATB by Transforming Growth Factor β1 (TGF-β1) Promotes Migration and Invasion of Papillary Thyroid Carcinoma Cells. *Med. Sci. Monit.* **2018**, *24*, 5152–5158. [CrossRef] [PubMed]
24. Goedert, L.; Plaça, J.R.; Fuziwara, C.S.; Machado, M.C.R.; Plaça, D.R.; Almeida, P.P.; Sanches, T.P.; Dos Santos, J.F.; Corveloni, A.C.; Pereira, I.E.G.; et al. Identification of Long Noncoding RNAs Deregulated in Papillary Thyroid Cancer and Correlated with BRAF V600E Mutation by Bioinformatics Integrative Analysis. *Sci. Rep.* **2017**, *7*, 1662. [CrossRef] [PubMed]
25. Qi, P.; Zhou, X.-Y.; Du, X. Circulating Long Non-Coding RNAs in Cancer: Current Status and Future Perspectives. *Mol. Cancer* **2016**, *15*, 39. [CrossRef]
26. Lan, X.; Zhang, H.; Wang, Z.; Dong, W.; Sun, W.; Shao, L.; Zhang, T.; Zhang, D. Genome-Wide Analysis of Long Noncoding RNA Expression Profile in Papillary Thyroid Carcinoma. *Gene* **2015**, *569*, 109–117. [CrossRef]
27. Yang, M.; Tian, J.; Guo, X.; Yang, Y.; Guan, R.; Qiu, M.; Li, Y.; Sun, X.; Zhen, Y.; Zhang, Y.; et al. Long Noncoding RNA Are Aberrantly Expressed in Human Papillary Thyroid Carcinoma. *Oncol. Lett.* **2016**, *12*, 544–552. [CrossRef]
28. Xu, B.; Shao, Q.; Xie, K.; Zhang, Y.; Dong, T.; Xia, Y.; Tang, W. The Long Non-Coding RNA ENST00000537266 and ENST00000426615 Influence Papillary Thyroid Cancer Cell Proliferation and Motility. *Cell. Physiol. Biochem.* **2016**, *38*, 368–378. [CrossRef]
29. Li, T.; Yang, X.-D.; Ye, C.-X.; Shen, Z.-L.; Yang, Y.; Wang, B.; Guo, P.; Gao, Z.-D.; Ye, Y.-J.; Jiang, K.-W.; et al. Long Noncoding RNA HIT000218960 Promotes Papillary Thyroid Cancer Oncogenesis and Tumor Progression by Upregulating the Expression of High Mobility Group AT-Hook 2 (HMGA2) Gene. *Cell Cycle* **2017**, *16*, 224–231. [CrossRef]
30. Vickers, K.C.; Roteta, L.A.; Hucheson-Dilks, H.; Han, L.; Guo, Y. Mining Diverse Small RNA Species in the Deep Transcriptome. *Trends Biochem. Sci.* **2015**, *40*, 4–7. [CrossRef]
31. Han, L.; Vickers, K.C.; Samuels, D.C.; Guo, Y. Alternative Applications for Distinct RNA Sequencing Strategies. *Brief. Bioinform.* **2015**, *16*, 629–639. [CrossRef] [PubMed]
32. Liyanarachchi, S.; Li, W.; Yan, P.; Bundschuh, R.; Brock, P.; Senter, L.; Ringel, M.D.; de la Chapelle, A.; He, H. Genome-Wide Expression Screening Discloses Long Noncoding RNAs Involved in Thyroid Carcinogenesis. *J. Clin. Endocrinol. Metab.* **2016**, *101*, 4005–4013. [CrossRef] [PubMed]

33. Wang, Q.; Yang, H.; Wu, L.; Yao, J.; Meng, X.; Jiang, H.; Xiao, C.; Wu, F. Identification of Specific Long Non-Coding RNA Expression: Profile and Analysis of Association with Clinicopathologic Characteristics and BRAF Mutation in Papillary Thyroid Cancer. *Thyroid* **2016**, *26*, 1719–1732. [CrossRef] [PubMed]
34. Ma, B.; Liao, T.; Wen, D.; Dong, C.; Zhou, L.; Yang, S.; Wang, Y.; Ji, Q. Corrigendum: Long Intergenic Non-Coding RNA 271 Is Predictive of a Poorer Prognosis of Papillary Thyroid Cancer. *Sci. Rep.* **2017**, *7*, 42321. [CrossRef] [PubMed]
35. Luo, Y.-H.; Liang, L.; He, R.-Q.; Wen, D.-Y.; Deng, G.-F.; Yang, H.; He, Y.; Ma, W.; Cai, X.-Y.; Chen, J.-Q.; et al. RNA-Sequencing Investigation Identifies an Effective Risk Score Generated by Three Novel lncRNAs for the Survival of Papillary Thyroid Cancer Patients. *Oncotarget* **2017**, *8*, 74139–74158. [CrossRef]
36. Zhao, W.; He, X.; Hoadley, K.A.; Parker, J.S.; Hayes, D.N.; Perou, C.M. Comparison of RNA-Seq by Poly (A) Capture, Ribosomal RNA Depletion, and DNA Microarray for Expression Profiling. *BMC Genom.* **2014**, *15*, 419. [CrossRef]
37. Guo, Y.; Zhao, S.; Sheng, Q.; Guo, M.; Lehmann, B.; Pietenpol, J.; Samuels, D.C.; Shyr, Y. RNAseq by Total RNA Library Identifies Additional RNAs Compared to Poly(A) RNA Library. *BioMed Res. Int.* **2015**, *2015*, 862130. [CrossRef]
38. O'Connell, T.J.; Dadafarin, S.; Jones, M.; Rodríguez, T.; Gupta, A.; Shin, E.; Moscatello, A.; Iacob, C.; Islam, H.; Tiwari, R.K.; et al. Androgen Activity Is Associated With PD-L1 Downregulation in Thyroid Cancer. *Front. Cell Dev. Biol.* **2021**, *9*, 663130. [CrossRef]
39. Zhou, Y.; Zhang, X.; Klibanski, A. MEG3 Noncoding RNA: A Tumor Suppressor. *J. Mol. Endocrinol.* **2012**, *48*, R45–R53. [CrossRef]
40. Ying, L.; Huang, Y.; Chen, H.; Wang, Y.; Xia, L.; Chen, Y.; Liu, Y.; Qiu, F. Downregulated MEG3 Activates Autophagy and Increases Cell Proliferation in Bladder Cancer. *Mol. Biosyst.* **2013**, *9*, 407–411. [CrossRef]
41. Harrow, J.; Frankish, A.; Gonzalez, J.M.; Tapanari, E.; Diekhans, M.; Kokocinski, F.; Aken, B.L.; Barrell, D.; Zadissa, A.; Searle, S.; et al. GENCODE: The Reference Human Genome Annotation for The ENCODE Project. *Genome Res.* **2012**, *22*, 1760–1774. [CrossRef] [PubMed]
42. Benlloch, S.; Payá, A.; Alenda, C.; Bessa, X.; Andreu, M.; Jover, R.; Castells, A.; Llor, X.; Aranda, F.I.; Massutí, B. Detection of BRAF V600E Mutation in Colorectal Cancer: Comparison of Automatic Sequencing and Real-Time Chemistry Methodology. *J. Mol. Diagn.* **2006**, *8*, 540–543. [CrossRef] [PubMed]
43. Langfelder, P.; Horvath, S. WGCNA: An R Package for Weighted Correlation Network Analysis. *BMC Bioinform.* **2008**, *9*, 559. [CrossRef] [PubMed]
44. Zhang, B.; Horvath, S. A General Framework for Weighted Gene Co-Expression Network Analysis. *Stat. Appl. Genet. Mol. Biol.* **2005**, *4*, 1–45. [CrossRef]
45. Liberzon, A.; Birger, C.; Thorvaldsdóttir, H.; Ghandi, M.; Mesirov, J.P.; Tamayo, P. The Molecular Signatures Database (MSigDB) Hallmark Gene Set Collection. *Cell Syst.* **2015**, *1*, 417–425. [CrossRef]
46. Goldman, M.; Craft, B.; Brooks, A.; Zhu, J.; Haussler, D. The UCSC Xena Platform for Cancer Genomics Data Visualization and Interpretation. *BioRxiv* **2018**, 326470. [CrossRef]
47. Cancer Genome Atlas Research Network. Integrated Genomic Characterization of Papillary Thyroid Carcinoma. *Cell* **2014**, *159*, 676–690. [CrossRef]
48. Pratilas, C.A.; Taylor, B.S.; Ye, Q.; Viale, A.; Sander, C.; Solit, D.B.; Rosen, N. V600EBRAF Is Associated with Disabled Feedback Inhibition of RAF–MEK Signaling and Elevated Transcriptional Output of the Pathway. *Proc. Natl. Acad. Sci. USA* **2009**, *106*, 4519–4524. [CrossRef]
49. Li, T.; Fu, J.; Zeng, Z.; Cohen, D.; Li, J.; Chen, Q.; Li, B.; Liu, X.S. TIMER2.0 for Analysis of Tumor-Infiltrating Immune Cells. *Nucleic Acids Res.* **2020**, *48*, W509–W514. [CrossRef]
50. Gao, R.; Bai, S.; Henderson, Y.C.; Lin, Y.; Schalck, A.; Yan, Y.; Kumar, T.; Hu, M.; Sei, E.; Davis, A.; et al. Delineating Copy Number and Clonal Substructure in Human Tumors from Single-Cell Transcriptomes. *Nat. Biotechnol.* **2021**, *39*, 599–608. [CrossRef]
51. Zeng, J.; Zhang, Y.; Shang, Y.; Mai, J.; Shi, S.; Lu, M.; Bu, C.; Zhang, Z.; Zhang, Z.; Li, Y.; et al. CancerSCEM: A Database of Single-Cell Expression Map across Various Human Cancers. *Nucleic Acids Res.* **2022**, *50*, D1147–D1155. [CrossRef] [PubMed]
52. Nikiforova, M.N.; Kimura, E.T.; Gandhi, M.; Biddinger, P.W.; Knauf, J.A.; Basolo, F.; Zhu, Z.; Giannini, R.; Salvatore, G.; Fusco, A.; et al. BRAF Mutations in Thyroid Tumors Are Restricted to Papillary Carcinomas and Anaplastic or Poorly Differentiated Carcinomas Arising from Papillary Carcinomas. *J. Clin. Endocrinol. Metab.* **2003**, *88*, 5399–5404. [CrossRef] [PubMed]
53. Xing, M.; Alzahrani, A.S.; Carson, K.A.; Viola, D.; Elisei, R.; Bendlova, B.; Yip, L.; Mian, C.; Vianello, F.; Tuttle, R.M.; et al. Association between BRAF V600E Mutation and Mortality in Patients with Papillary Thyroid Cancer. *JAMA* **2013**, *309*, 1493–1501. [CrossRef] [PubMed]
54. Yoo, S.-K.; Lee, S.; Kim, S.-J.; Jee, H.-G.; Kim, B.-A.; Cho, H.; Song, Y.S.; Cho, S.W.; Won, J.-K.; Shin, J.-Y.; et al. Comprehensive Analysis of the Transcriptional and Mutational Landscape of Follicular and Papillary Thyroid Cancers. *PLoS Genet.* **2016**, *12*, e1006239. [CrossRef]
55. Song, Y.S.; Won, J.-K.; Yoo, S.-K.; Jung, K.C.; Kim, M.J.; Kim, S.-J.; Cho, S.W.; Lee, K.E.; Yi, K.H.; Seo, J.-S.; et al. Comprehensive Transcriptomic and Genomic Profiling of Subtypes of Follicular Variant of Papillary Thyroid Carcinoma. *Thyroid* **2018**, *28*, 1468–1478. [CrossRef]
56. Hamatani, K.; Eguchi, H.; Koyama, K.; Mukai, M.; Nakachi, K.; Kusunoki, Y. A Novel RET Rearrangement (ACBD5/RET) by Pericentric Inversion, Inv (10)(p12. 1; q11. 2), in Papillary Thyroid Cancer from an Atomic Bomb Survivor Exposed to High-Dose Radiation. *Oncol. Rep.* **2014**, *32*, 1809–1814. [CrossRef]
57. Greco, A.; Miranda, C.; Pierotti, M.A. Rearrangements of NTRK1 Gene in Papillary Thyroid Carcinoma. *Mol. Cell. Endocrinol.* **2010**, *321*, 44–49. [CrossRef]

58. Tsai, M.-C.; Manor, O.; Wan, Y.; Mosammaparast, N.; Wang, J.K.; Lan, F.; Shi, Y.; Segal, E.; Chang, H.Y. Long Noncoding RNA as Modular Scaffold of Histone Modification Complexes. *Science* **2010**, *329*, 689–693. [CrossRef]
59. Nikiforov, Y.E.; Carty, S.E.; Chiosea, S.I.; Coyne, C.; Duvvuri, U.; Ferris, R.L.; Gooding, W.E.; LeBeau, S.O.; Ohori, N.P.; Seethala, R.R.; et al. Impact of the Multi-Gene ThyroSeq Next-Generation Sequencing Assay on Cancer Diagnosis in Thyroid Nodules with Atypia of Undetermined Significance/Follicular Lesion of Undetermined Significance Cytology. *Thyroid* **2015**, *25*, 1217–1223. [CrossRef]
60. Kim, T.H.; Park, Y.J.; Lim, J.A.; Ahn, H.Y.; Lee, E.K.; Lee, Y.J.; Kim, K.W.; Hahn, S.K.; Youn, Y.K.; Kim, K.H.; et al. The Association of the BRAFV600E Mutation with Prognostic Factors and Poor Clinical Outcome in Papillary Thyroid Cancer: A Meta-Analysis. *Cancer* **2012**, *118*, 1764–1773. [CrossRef]
61. Xu, T.-P.; Ma, P.; Wang, W.-Y.; Shuai, Y.; Wang, Y.-F.; Yu, T.; Xia, R.; Shu, Y.-Q. KLF5 and MYC Modulated LINC00346 Contributes to Gastric Cancer Progression through Acting as a Competing Endogeous RNA and Indicates Poor Outcome. *Cell Death Differ.* **2019**, *26*, 2179–2193. [CrossRef] [PubMed]
62. Lessard, L.; Liu, M.; Marzese, D.M.; Wang, H.; Chong, K.; Kawas, N.; Donovan, N.C.; Kiyohara, E.; Hsu, S.; Nelson, N.; et al. The CASC15 Long Intergenic Noncoding RNA Locus Is Involved in Melanoma Progression and Phenotype Switching. *J. Investig. Dermatol.* **2015**, *135*, 2464–2474. [CrossRef] [PubMed]
63. Wang, A.; Bao, Y.; Wu, Z.; Zhao, T.; Wang, D.; Shi, J.; Liu, B.; Sun, S.; Yang, F.; Wang, L.; et al. Long Noncoding RNA EGFR-AS1 Promotes Cell Growth and Metastasis via Affecting HuR Mediated mRNA Stability of EGFR in Renal Cancer. *Cell Death Dis.* **2019**, *10*, 154. [CrossRef] [PubMed]
64. Cui, K.; Jin, S.; Du, Y.; Yu, J.; Feng, H.; Fan, Q.; Ma, W. Long Noncoding RNA DIO3OS Interacts with miR-122 to Promote Proliferation and Invasion of Pancreatic Cancer Cells through Upregulating ALDOA. *Cancer Cell Int.* **2019**, *19*, 202. [CrossRef] [PubMed]
65. Pandey, G.K.; Mitra, S.; Subhash, S.; Hertwig, F.; Kanduri, M.; Mishra, K.; Fransson, S.; Ganeshram, A.; Mondal, T.; Bandaru, S.; et al. The Risk-Associated Long Noncoding RNA NBAT-1 Controls Neuroblastoma Progression by Regulating Cell Proliferation and Neuronal Differentiation. *Cancer Cell* **2014**, *26*, 722–737. [CrossRef] [PubMed]
66. Wang, C.; Yan, G.; Zhang, Y.; Jia, X.; Bu, P. Long Non-Coding RNA MEG3 Suppresses Migration and Invasion of Thyroid Carcinoma by Targeting of Rac1. *Neoplasma* **2015**, *62*, 541–549. [CrossRef]
67. Joyce, J.A. Therapeutic Targeting of the Tumor Microenvironment. *Cancer Cell* **2005**, *7*, 513–520. [CrossRef]
68. Mao, Y.; Keller, E.T.; Garfield, D.H.; Shen, K.; Wang, J. Stromal Cells in Tumor Microenvironment and Breast Cancer. *Cancer Metastasis Rev.* **2013**, *32*, 303–315. [CrossRef]
69. Molinaro, E.; Romei, C.; Biagini, A.; Sabini, E.; Agate, L.; Mazzeo, S.; Materazzi, G.; Sellari-Franceschini, S.; Ribechini, A.; Torregrossa, L.; et al. Anaplastic Thyroid Carcinoma: From Clinicopathology to Genetics and Advanced Therapies. *Nat. Rev. Endocrinol.* **2017**, *13*, 644–660. [CrossRef]
70. Mondal, T.; Subhash, S.; Vaid, R.; Enroth, S.; Uday, S.; Reinius, B.; Mitra, S.; Mohammed, A.; James, A.R.; Hoberg, E.; et al. MEG3 Long Noncoding RNA Regulates the TGF-β Pathway Genes through Formation of RNA-DNA Triplex Structures. *Nat. Commun.* **2015**, *6*, 7743. [CrossRef]
71. Kameyama, K. Expression of MMP-1 in the Capsule of Thyroid Cancer—Relationship with Invasiveness. *Pathol. Res. Pract.* **1996**, *192*, 20–26. [CrossRef]
72. Ren, L.; Xu, Y.; Liu, C.; Wang, S.; Qin, G. IL-17RB Enhances Thyroid Cancer Cell Invasion and Metastasis via ERK1/2 Pathway-Mediated MMP-9 Expression. *Mol. Immunol.* **2017**, *90*, 126–135. [CrossRef] [PubMed]
73. Shen, Z.; Wang, X.; Yu, X.; Zhang, Y.; Qin, L. MMP16 Promotes Tumor Metastasis and Indicates Poor Prognosis in Hepatocellular Carcinoma. *Oncotarget* **2017**, *8*, 72197–72204. [CrossRef]
74. Hwang, H.S.; Orloff, L.A. Efficacy of Preoperative Neck Ultrasound in the Detection of Cervical Lymph Node Metastasis from Thyroid Cancer. *Laryngoscope* **2011**, *121*, 487–491. [CrossRef] [PubMed]
75. Stulak, J.M.; Grant, C.S.; Farley, D.R.; Thompson, G.B.; van Heerden, J.A.; Hay, I.D.; Reading, C.C.; Charboneau, J.W. Value of Preoperative Ultrasonography in the Surgical Management of Initial and Reoperative Papillary Thyroid Cancer. *Arch. Surg.* **2006**, *141*, 489–494, discussion 494–496. [CrossRef]
76. Prensner, J.R.; Iyer, M.K.; Sahu, A.; Asangani, I.A.; Cao, Q.; Patel, L.; Vergara, I.A.; Davicioni, E.; Erho, N.; Ghadessi, M.; et al. The Long Noncoding RNA SChLAP1 Promotes Aggressive Prostate Cancer and Antagonizes the SWI/SNF Complex. *Nat. Genet.* **2013**, *45*, 1392–1398. [CrossRef]
77. Gutschner, T.; Diederichs, S. The Hallmarks of Cancer: A Long Non-Coding RNA Point of View. *RNA Biol.* **2012**, *9*, 703–719. [CrossRef]
78. Zhang, S.; Guo, W. Long Non-coding RNA MEG3 Suppresses the Growth of Glioma Cells by Regulating the miR-96-5p/MTSS1 Signaling Pathway. *Mol. Med. Rep.* **2019**, *20*, 4215–4225. [CrossRef]
79. Liu, Z.; Chen, J.Y.; Zhong, Y.; Xie, L.; Li, J.S. lncRNA MEG3 Inhibits the Growth of Hepatocellular Carcinoma Cells by Sponging miR-9-5p to Upregulate SOX11. *Braz. J. Med. Biol. Res.* **2019**, *52*, e8631. [CrossRef]
80. Pan, H.; Diao, H.; Zhong, W.; Wang, T.; Wen, P.; Wu, C. A Cancer Cell Cluster Marked by LincRNA MEG3 Leads Pancreatic Ductal Adenocarcinoma Metastasis. *Front. Oncol.* **2021**, *11*, 656564. [CrossRef]
81. Miyazono, K. Positive and Negative Regulation of TGF-Beta Signaling. *J. Cell Sci.* **2000**, *113 Pt 7*, 1101–1109. [CrossRef] [PubMed]

82. Terashima, M.; Tange, S.; Ishimura, A.; Suzuki, T. MEG3 Long Noncoding RNA Contributes to the Epigenetic Regulation of Epithelial-Mesenchymal Transition in Lung Cancer Cell Lines. *J. Biol. Chem.* **2017**, *292*, 82–99. [CrossRef] [PubMed]
83. Gokey, J.J.; Snowball, J.; Sridharan, A.; Speth, J.P.; Black, K.E.; Hariri, L.P.; Perl, A.-K.T.; Xu, Y.; Whitsett, J.A. MEG3 Is Increased in Idiopathic Pulmonary Fibrosis and Regulates Epithelial Cell Differentiation. *JCI Insight* **2018**, *3*, 122490. [CrossRef] [PubMed]
84. Aran, D.; Camarda, R.; Odegaard, J.; Paik, H.; Oskotsky, B.; Krings, G.; Goga, A.; Sirota, M.; Butte, A.J. Comprehensive Analysis of Normal Adjacent to Tumor Transcriptomes. *Nat. Commun.* **2017**, *8*, 1077. [CrossRef]